

Lattice Boltzmann modeling of buoyant rise of single and multiple bubbles

Shadab Anwar*

Geological Sciences & Engineering, Missouri University of Science & Technology, 129 McNutt Hall, 1400 N. Bishop, Rolla, MO 65409, USA



ARTICLE INFO

Article history:

Received 7 March 2013

Received in revised form 10 September 2013

Accepted 12 September 2013

Available online 25 September 2013

Keywords:

Bubble dynamics

Lattice Boltzmann method

Terminal velocity

ABSTRACT

Buoyant rise of bubbles is investigated using the lattice Boltzmann method (LBM) based Gunstensen's color model. An external force/sink term is incorporated in the collision step to simulate buoyant rise of bubbles under gravitational force. The shape of a bubble is controlled by inertial, viscous and surface tension forces. The interplay between these forces is quantified using non-dimensional numbers such as Eötvös number (Eo), Morton number (Mo) and Reynolds number (Re). A set of results from numerical simulations are presented to demonstrate the ability of the proposed approach to simulate rise of single and multiple bubbles under buoyancy. The proposed modification is verified by comparing terminal velocity of bubbles in an infinite medium against the analytical solution. The shape of bubbles in various flow regimes characterized by the non-dimensional numbers is compared against the experimental data. The effect of surface tension and viscosity ratio on terminal velocity and shape of bubbles is investigated. The LBM results for topological change in the shape of bubbles or circularity of bubbles is compared against COMSOL. Co-axial and oblique coalescence of two gas bubbles are simulated and compared against the experimental data. The simulation results from LBM simulations were found to be in good agreement with the analytical solution, the experimental data and the COMSOL simulation.

© 2013 Elsevier Ltd. All rights reserved.

1. Introduction

Multiphase flow system is commonly observed in several natural and industrial processes such as ink-jet printing [1,2], spray cooling [3,4], carbon sequestration [5], soil-vapor extraction [6–8] and nuclear waste management [9,10]. Buoyant rise of bubbles under gravitational force has been a common area of interest for experimental and numerical researchers. Rise of bubbles in viscous fluid is characterized by non-dimensional numbers such as the Eötvös number $Eo = \frac{d_0^2 g \Delta \rho}{\sigma}$, Morton number $Mo = \frac{\rho_l^2 v_l^4 g \Delta \rho}{\sigma^3}$ and Reynolds number $Re = \frac{v_l d_0}{\nu_l}$; where d_0 is diameter of bubble, ρ_l is density of suspended liquid, and ρ_g is density of gas or bubble, ν_l is kinematic viscosity of liquid, $\Delta \rho = \rho_l - \rho_g$ is the density difference between the liquid (ρ_l) and the gas/bubble (ρ_g), g is gravitational acceleration, V is terminal velocity and σ is surface tension. Eötvös number (Eo) and Morton number (Mo) represent the ratio between surface tension force and buoyant force acting on a suspended bubble. Reynolds number (Re) indicates the balance between viscous drag and inertial force. Buoyant force lifts the bubble against the gravity whereas the viscous drag tends to retard the flow of a

bubble. Surface tension force tries to maintain the spherical shape of a bubble.

Different numerical methods have been applied to simulate multiphase flow (see Prosperetti and Tryggvason [11]). Fuster, Agbaglah [12] used a volume of fluid (VOF) method, balanced-force surface tension and quad/octree adaptive mesh refinement (AMR) to simulate bubble dynamics. van Sint Annaland et al. [13] presented an interface reconstruction technique based on piecewise linear interface representation in volume of fluid (VOF) method to simulate co-axial and oblique coalescence of two gas bubbles. van Sint Annaland et al. [14] used a 3-D front tracking method employing a new surface tension model to simulate single and multiple bubble dynamics in dispersed fluid. Olsson and Kreiss [15–17] used a level set method to simulate bubble dynamics. COMSOL Multiphysics [18] is a commercial software that applies level set method to simulate multiphase flow system.

The numerical simulation of multiphase flow is a challenging class of problems because of the inherent difficulty in tracking the fluid interfaces, mass conservation, and the correct treatment of the surface tension forces [19]. In recent years, the lattice Boltzmann method (LBM) has emerged as a very promising numerical approach for simulation of complex multiphase flow [20–26]. LBM based immiscible multiphase flow model can be divided into three types: Rothman–Keller (R–K) model [20,27,28], the Shan–Chen (SC) model [22], and the free energy (FE) approach

* Tel.: +1 (573) 341 4466; fax: +1 (573) 341 6935.

E-mail address: anwarsh@mst.edu

[24,29]. Huang et al. [30] compared performance and stability of three approaches to simulate immiscible multiphase flow; the FE method was found to be better than the other two approaches for high density and viscosity contrast between two fluid components.

Sankaranarayanan et al. [31] presented comparison between LBM and front-tracking finite-difference methods for bubble simulations and found that both numerical schemes are qualitatively similar and within a few percent quantitatively. Several variants of LBM based multiphase flow model [19,32–39] have been applied to simulate bubble dynamics in recent years. The successes of LBM-based simulations are mainly due to their mesoscopic and kinetic nature, which enables the simulation of their macroscopic interfacial dynamics with their underlying microscopic nature.

In this work, we adopted the Rothman–Keller (R–K) type binary color model introduced by Gunstensen [20,27] for the LBM to simulate immiscible multiphase flow. The Gunstensen's binary color model recovers Galilean invariance with proper assignment of immobile equilibrium particle, and the model can adjust the surface tension independent of the density and the viscosity contrast between binary fluid components [40]. However, the model works well only for negligible density ratios [39,41], and is computationally less efficient than the Shan–Chen model [22] due to an additional collision step for perturbation (see detail in the following section). Grunau et al. [42] introduced two real valued parameters in the original binary color model to account for density contrast between two fluid components. Tölke [33] applied Gunstensen's color model with modification suggested by Grunau et al. [42] to simulate multicomponent multiphase flow in porous media with variable density and viscosity ratios between multiple binary fluids. It was found that the model is not stable for large-scale real-life problems where binary fluids have significant density or viscosity contrast. The binary color model has been applied to demonstrate the effect of geometry and viscosity contrast on flow regimes at high capillary numbers [34,41]. Farhat et al. [43] applied binary color model to simulate deformation and velocity of red blood cell (RBC) while streaming through capillaries whose diameters are smaller than the RBC size. The interfacial surface tension was made non-uniform as a function of surfactant concentration on RBC. Leclaire et al. [44] modified the original recoloring step proposed by Latva-Kokko and Rothman [45] in Gunstensen's binary color model to improve efficiency and accuracy of estimate for surface tension. The modified model is able to simulate viscosity contrast as high as 10,000. Tölke et al. [40] applied Gunstensen's color model on multiple relaxation time (MRT) scheme in LBM to simulate multi-phase flows on non-uniform adaptive grids. Li et al. [46] modified Gunstensen's color model on the MRT scheme by decoupling the interfacial tension and the viscosity-related relaxation time, and adding another MRT diffusion step to eliminate the anti-diffusion effect of the recoloring step.

Bubble dynamics have been studied using different variants of LBM-based multiphase flow model. Sankaranarayanan et al. [47] used both the Shan and Chen [22] and the Shan and Doolen [23] multiphase models to simulate bubble dynamics for a density ratio of 100 with $Bo < 5$ and $Mo > 1 \times 10^{-6}$ [19,32] have used the Shan–Chen model to simulate bubble dynamics. A non-ideal equation of state is generally assumed in this model to implement the interfacial surface tension, and an external forcing term [47] was used to implement buoyancy effect in the multiphase flow model. Yu and Fan [48] applied the adaptive mesh refinement (AMR) method on the Shan–Chen model to simulate buoyant rise of bubbles and found that LBM combined with AMR can significantly improve accuracy and reduce computational cost [36,37] have applied free energy (FE) method [24] to study dynamics of single bubbles for moderate Reynolds number [21,49,50] used the projection method in the free energy (FE) method to simulate buoyant rise of bubble

for high density ratio. Zheng et al. [51] included external forcing term [37] in the free energy (FE) method to simulate bubble dynamics with large density ratio. Farhat et al. [39] have combined 3-D migrating multi-block algorithm with Gunstensen's color model to study bubble dynamics. The Grunau et al. [42] method was adopted in this model to simulate density contrast; however, the highest density contrast applied was $O(10)$ due to thick interface between the two fluids and stability issues.

The objective of this paper is to present a modification in the LBM-based Gunstensen's color model [20] to simulate buoyant rise of bubbles. An effective force term is included during the collision step in the model to account for buoyant force due to density contrast between the fluid components; hence, the buoyancy was not directly simulated as an effect of pressure gradients in the flow, but was introduced from an analytical understanding of buoyancy effects. Therefore, density contrast was not explicitly introduced in the model. Mohamad and Kuzmin [52] explored three different schemes to implement external force in LBM to simulate physical processes such as density dependent flow, as well as spatially and/or temporally varying body force with non-zero gradients. Buick and Greated [53] also analyzed the implementation of body force in LBM and concluded that better accuracy in LBM can be achieved by adding external force in the collision step. This work verifies the shape regime obtained with the proposed modification at various Eo and Mo numbers against the experimental data. The terminal velocity for bubbles from LBM simulation was verified against the analytical solution, and the LBM results were also compared against COMSOL simulation for circularity of bubble and terminal Re . The simulation results from LBM for oblique and co-axial coalescence of two bubbles were compared against the experimental data.

2. Lattice Boltzmann model

Lattice Boltzmann method (LBM) is a numerical scheme to simulate hydrodynamic systems governed by the Navier–Stokes equations (NSE) for isothermal compressible fluid flow [1,54,55]. LBM's are based on kinetic theory of gas at microscopic scale and have proven to recover the Navier–Stokes solution at macroscopic scales through Chapman–Enskog expansion of the Boltzmann equation at low frequency, long wavelength limits, and at a low Mach number [56]. Mach number (Ma) is a non-dimensional number that represents velocity of fluid (V) relative to speed of sound (c_s). Unlike traditional numerical methods, the LBM does not discretize the governing equations at macroscopic scale in space and time; instead, it solves the dynamics of hypothetical particles governed by the Boltzmann equation. The Boltzmann equation governs the time rate of change of the particle distribution function (f_j). The particle distribution function (f_j) represents the dynamic state of a hypothetical group of particles in terms of its location (\mathbf{x}) and momentum at any time (t). The f_j streams on discrete lattices and is updated by a collision mechanism.

The linearized discrete Boltzmann equation as shown in Eq. (1) is solved on discrete lattices [56]:

$$\underbrace{f'_j(\mathbf{x} + \mathbf{e}_j \Delta t, t + \Delta t)}_{\text{Streaming}} = \underbrace{f_j(\mathbf{x}, t) - \frac{f_j(\mathbf{x}, t) - f_j^{eq}(\mathbf{x}, t)}{\tau}}_{\text{Collision}} + \varphi_j \quad (1)$$

where \mathbf{e}_j is the microscopic velocity of particle groups, f_j^{eq} is equilibrium distribution function and τ is a relaxation parameter that indicates the rate at which the system approaches equilibrium through a series of collisions and streaming. φ_j is a sink term that will be

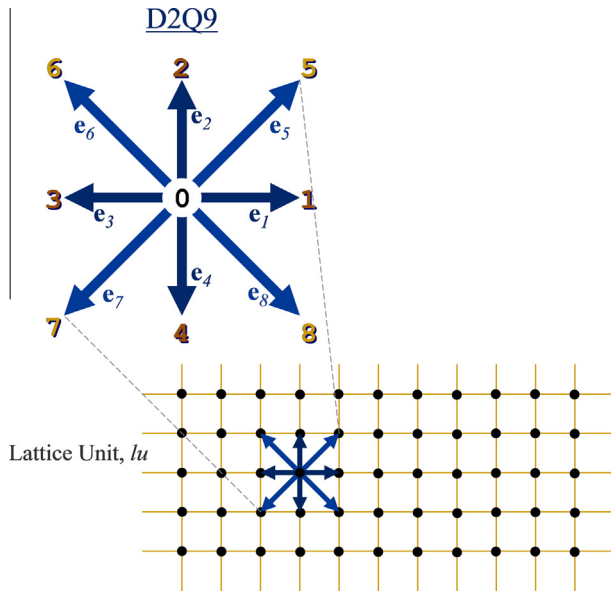


Fig. 1. Schematic of a numerical grid and definition of lattice space unit (lu), and unit velocities for streaming step in D2Q9 model [70].

used to implement the interfacial surface tension and the buoyancy effect. The macroscopic properties such as density (ρ) and macroscopic velocity (\mathbf{u}) are calculated as [56]:

$$\rho = \sum_{j=0}^8 f_j \quad (2)$$

$$\mathbf{u} = \frac{1}{\rho} \sum_{j=0}^8 f_j \mathbf{e}_j \quad (3)$$

We used a 2-D model called D2Q9 in LBM with $j = 9$ discrete set of particle groups with discrete particle velocity (\mathbf{e}_j) (see Fig. 1).

The linearized discrete Boltzmann equation with Bhatnagar–Gross–Krook (BGK) type collision [57], as shown in Eq. (1), is solved on discrete lattices. The unique characteristic of BGK type collision is that there is only one relaxation parameter (τ) in contrast to the multiple relaxation time (MRT) model [3,4], which has more than one relaxation parameter to enhance the stability of LBM. The equilibrium distribution function f_j^{eq} for the Navier–Stokes equation (NSE) solver is [56]:

$$f_j^{eq} = w_j \rho \left(1 + \mathbf{e} \cdot \mathbf{u} + \frac{3}{2} (\mathbf{e} \cdot \mathbf{u})^2 - \frac{\mathbf{u}^2}{2} \right) \quad (4)$$

The weights w_j for a D2Q9 model are $1/3$ for $j = 1, 2, 3, 4$ (main Cartesian axes), and $1/12$ for $j = 5, 6, 7, 8$ (diagonals). The weight for remaining particles ($j = 0$) is $4/9$ [56]. The kinematic viscosity (ν) of fluid is controlled by the relaxation parameter τ , $\nu = c_s^2 \Delta t (\tau - \frac{1}{2})$; c_s is the speed of sound; $c_s = c/\sqrt{3}$ and $c = \Delta x/\Delta t$; where $\Delta x = 1$ lattice unit (lu), and $\Delta t = 1$ time step (ts), which are grid resolutions in space and time respectively. Lattice Boltzmann models can be thought of as having their own consistent set of dimensional units given in terms of lattice space units (lu), lattice time steps (ts), and lattice mass units (mu), which correspond to space (\mathbf{x}), time (t), and mass, respectively. To compare any physical system with any numerical simulation (e.g., LBM), it is convenient to relate the physical system and simulation by non-dimensional numbers such as Re, Eo and Mo. The pressure (p) in the LBM is calculated by the equation of state, $p = c_s^2 \rho$.

We implemented the LBM based binary color model [20] to simulate multiphase flow. Each fluid in a binary multiphase system was assigned a color, Red (R) or Blue (B), and each fluid component (col-

or) underwent streaming and collision processes as shown in Eq. (1). The standard Gunstensen's color model uses a color blind total particle distribution function which is the sum of two functions.

$$f_j(\mathbf{x}, t) = f_j^R(\mathbf{x}, t) + f_j^B(\mathbf{x}, t) \quad (5)$$

where f^R and f^B are distribution functions for red and blue phases. The density for each color phase (ρ^R and ρ^B) can be calculated using Eq. (2). Lishchuk et al. [58] introduced the perturbation step with a direct forcing term near the interface of the two fluid components. A local pressure gradient is introduced at the interface to implement the stress boundary condition and the continuity equation for the incompressible fluids. The force acts centripetally normal to the interface and is defined as [58]:

$$\rho^N(\mathbf{x}, t) = \frac{\rho^R(\mathbf{x}, t) - \rho^B(\mathbf{x}, t)}{\rho^R(\mathbf{x}, t) + \rho^B(\mathbf{x}, t)} \quad (6)$$

Hence, $-1 \leq \rho^N(\mathbf{x}, t) \leq 1$. The normal vector is used to calculate the local curvature at diffused interface. The normal vector is $\mathbf{n} = -\frac{\nabla \rho^N}{|\nabla \rho^N|}$. The radius of curvature (r) of the interface is computed

Table 1
Simulation parameters for different shapes of bubble in various flow regimes.

Case	Eo	Mo	Re	Shape
A2	116	266	4.1	Oblate ellipsoid cap
A4	116	5.51	14.7	Oblate ellipsoid cap
A6	116	0.103	49.3	Spherical cap closed wake
A7	116	4.6×10^{-3}	102.1	Spherical cap open wake
B2	17.7	711	0.32	Spherical
C1	5	3.2×10^{-4}	20.16	Oblate ellipsoidal
C2	1.56	7.36×10^{-4}	4.3	Spherical
C3	32	8.2×10^{-4}	22.3	Oblate ellipsoid disk

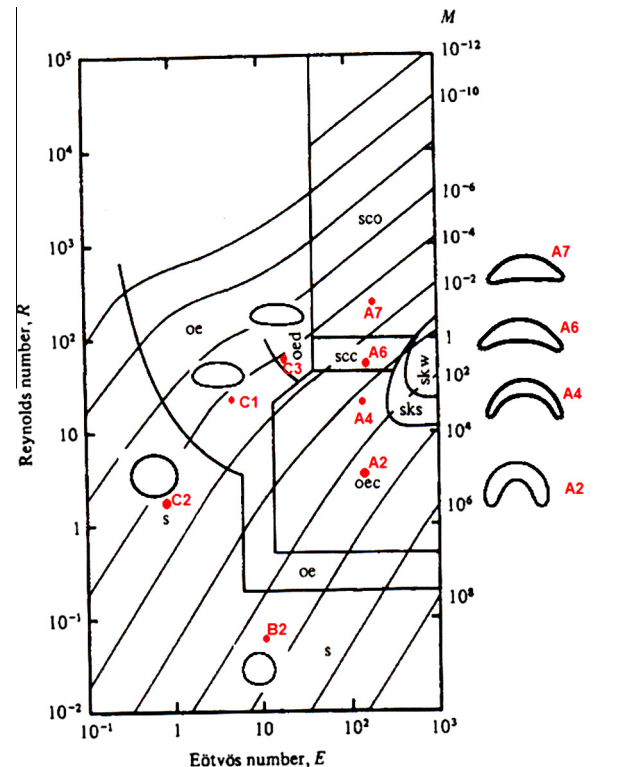


Fig. 2. The LB model results for the shape of bubble in three different regimes is compared against the laboratory data presented by Grace [60].

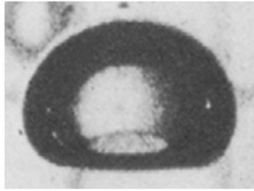
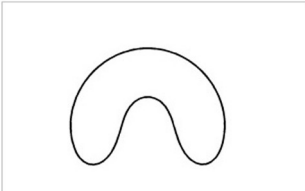
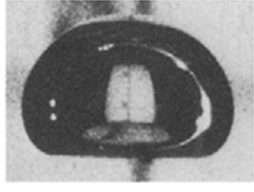
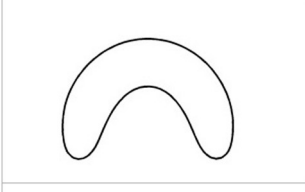



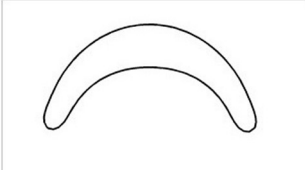
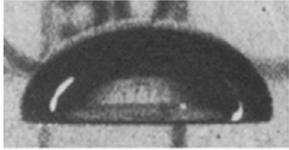
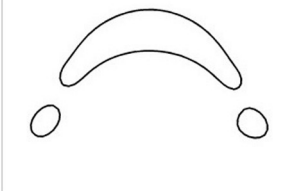
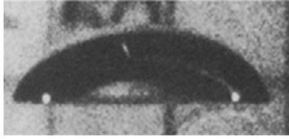
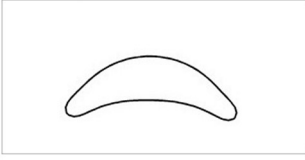
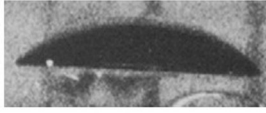


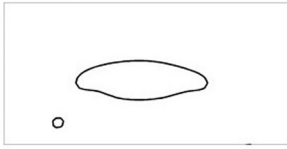
	Experiment		LBM
A1	Eo=116 M=848 Re=2.47		 Eo=116 M=848 Re=3.0
A2	Eo=116 M=266 Re=3.57		 Eo=116 M=266 Re=4.3
A3	Eo=116 M=41.1 Re=7.16		 Eo=116 M=41.1 Re=8.1
A4	Eo=116 Mo=5.51 Re=13.3		 Eo=116 Mo=5.51 Re=13.7
A5	Eo=116 Mo=1.31 Re=20.4		 Eo=116 Mo=1.31 Re=21.7
A6	Eo=116 Mo=0.103 Re=42.2		 Eo=116 Mo=0.103 Re=44.6
A7	Eo=116 Mo=4.6e-03 Re=94.0		 Eo=116 Mo=4.6e-03 Re=95.8
A8	Eo=116 Mo=8.6e-04 Re=151		 Eo=116 Mo=8.6e-04 Re=153.9

Fig. 3. Comparison of terminal bubble shapes observed in experiments [62] and predicted in simulation under difference conditions (A1–A8) of various Reynolds (Re), Morton (Mo) and Eötvös (Eo) numbers.

as $\kappa = \frac{1}{r} = -\nabla s \cdot \mathbf{n}$ and $\nabla s = (\mathbf{I} - \mathbf{nn}) \cdot \nabla$, where \mathbf{I} is the unit tensor and ∇s is the surface gradient operator. The source term φ_j , is used to implement interfacial surface tension and is calculated as:

$$\varphi_j = \frac{w_a}{c_s^2} \mathbf{F} \cdot \mathbf{e}_j \quad (7)$$

where $\mathbf{F}(\mathbf{x}, t) = \frac{1}{2r} \sigma \nabla \rho^N$; σ is surface tension. Latva-Kokko and Rothman [45] presented an improved segregation mechanism that can minimize the spurious velocities near the interface and also remove lattice pinning. The post-collision segregation of the two color phases is [45]:

$$f_j^R = \frac{\rho^R}{\rho^R + \rho^B} f_j + w_j \beta \frac{\rho^R \rho^B}{\rho^R + \rho^B} \cos \theta_f |\mathbf{e}_j| \quad (8)$$

$$f_j^B = \frac{\rho^B}{\rho^R + \rho^B} f_j - w_j \beta \frac{\rho^R \rho^B}{\rho^R + \rho^B} \cos \theta_f |\mathbf{e}_j| \quad (9)$$

where $\cos \theta_f = \frac{\mathbf{e}_j \cdot \nabla \rho^N}{|\mathbf{e}_j| |\nabla \rho^N|}$, β is a free parameter used to minimize the spurious currents and maintain a thin interface [45]. β is set equal to 0.7 for this work.

An effective buoyancy term φ_j is introduced in the collision step (Eq. (1)) to account for buoyancy force caused due to density difference ($\Delta\rho = \rho^R - \rho^B$) between the two color phases. The effective buoyancy term φ_j is [37,51,52,59]

$$\varphi_j = \frac{(\rho^R - \rho^B)}{8} \cdot \frac{e_{j,y}}{|e_{j,y}|} \cdot \frac{|\mathbf{g}| \Delta t}{c} \quad (10)$$

$e_{j,y}$ was the y-component of particle velocity in the j th direction (see Fig. 1). The effective buoyancy term was only applied on the gas/bubble phase. This approach of adding a force term in collision step allowed us to simulate a density dependent flow. The term $(\rho^R - \rho^B)g$ in Eq. (9) is same as $(\rho_l - \rho_g)g$ term in the non-dimensional number Eo and Mo ; hence, we were able to simulate a wide range of flow regimes using the proposed buoyancy model.

3. Results and discussion

We performed a series of 2-dimensional axis symmetric and one non-axis symmetric simulation using the LBM based Gunstensen's color model [20,27] combined with modifications suggested by Lishchuk et al. [58], and the proposed external forcing term (Eq. (9)). See Appendix A for the verification of LBM model against Laplace's law (A.1), low spurious velocity near the interface (A.2) and the verification of drag coefficient (A.3).

3.1. Terminal shape of bubble in different flow regimes

Grace [60], Clift et al. [61] and Bhaga and Weber [62] compiled laboratory data for shape regimes of single gas bubbles rising under gravity over a wide range of $Eo = O(1-10^3)$ and $Re = O(1-10^3)$. The observed shape of a bubble was plotted against Re and Eo as axes with isovalues of Mo . It was found that flow regimes have significant effect on the terminal shape of the bubbles. Terminal shape of bubbles was classified into three major types: spherical, ellipsoidal and spherical cap. The shape of bubbles remain spherical for low Reynolds or Eötvös number ($Re < 1$ or $Eo < 1$) and they rise in a steady fashion while maintaining their spherical shape. The shape of bubbles changed significantly since the flow regimes fall under intermediate Re and Eo numbers ($1 < Re < 100$ or $1 < Eo < 100$). It was observed during laboratory experiments that bubbles develop different terminal shapes (oblate ellipsoid, disk-like, oblate ellipsoidal cap, skirt bubble, and spherical-cap) in various flow regimes.

For better accuracy and to avoid wall effect in numerical simulation of buoyant rise of bubble in a bounded domain, the width and height of numerical domain should be $4d_0$ and $12d_0$ respectively [36,39,63]. The radial distance of boundary should be sufficiently far from the bubble to avoid any boundary effects, and an infinite extent of quiescent liquid can be assumed in the simulation. The domain for numerical simulation is 96 lu wide and 288 lu high and initial diameter (d_0) of bubble is 24 lu. The domain is bounded on all four sides, and a standard bounce-back scheme in LBM was adopted to implement no-slip boundary near the solid wall. The viscosity ratio ($\eta = \nu_l/\nu_g$) was 100. The simulation parameters in Table 1 are given for the LBM simulations to develop different terminal shapes of bubbles for different flow regimes as observed by Grace [60]. The bubble rises in a straight path under

different flow regimes. As the Reynolds number (Re) increases, turbulent wake develops behind the bubble that leads to an unsteady rise of bubbles. The bubbles may wobble, oscillate and even undergo break up or coalescence. The terminal shapes of bubbles from an LB model for different Eo , Re and Mo numbers are shown in Fig. 2. The proposed buoyancy model can produce a terminal shape (spherical, ellipsoidal, spherical cap, skirt-like) of bubbles in different flow regimes in agreement with experimental observations by Grace [60].

Table 2

Simulation parameters for verification of LB model against the analytical solution for terminal velocity of the bubble.

Gravity (g)	Eo	Mo	(Re) _{LBM}	V_{LBM}	$V_{analytical}$
3.6×10^{-4}	207	455	5.57	0.0316	0.03
4.5×10^{-4}	259	568	6.62	0.0368	0.0359
5.4×10^{-4}	311	682	7.32	0.0407	0.04
6.5×10^{-4}	374	821	7.93	0.0441	0.0444
7.8×10^{-4}	449	985	8.55	0.0475	0.049

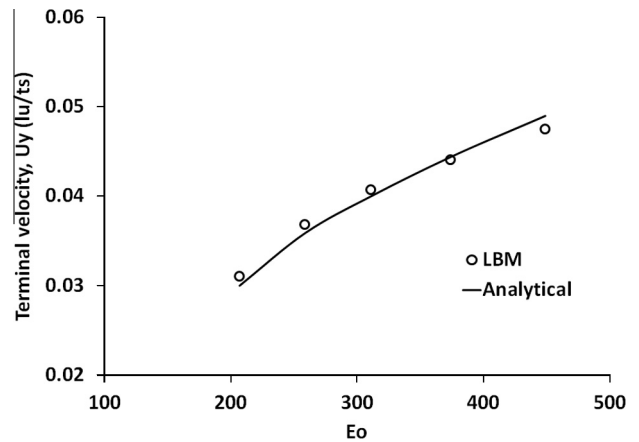


Fig. 4. Comparison between LB model data and analytical solution for terminal velocity. Parameters for the simulation in given in Table 2.

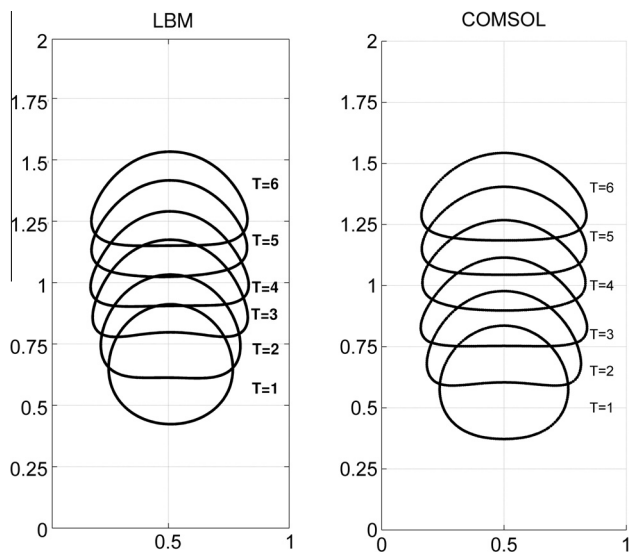


Fig. 5. Change in shape of bubble at $Eo = 9$ and $Mo = 6e-04$. The evolution of bubble obtained from LBM (left) is compared against the bubble shape developed by COMSOL simulation [32].

The terminal shape of bubbles from LBM simulation was compared against the shape of bubbles observed in laboratory experiments for different Eo and Re numbers. The proposed model can simulate topological changes in shape of bubbles for different Eo and Mo numbers. The comparison between LBM results for the terminal shape of bubbles and experimental observations as presented by Bhaga and Weber [62] are shown in Fig. 3. The non-

dimensional numbers used in experiment and simulations are shown in both the left and right columns in Fig. 3. The observed shape of bubbles is shown in the third column, and the shape of bubbles from the LBM simulation is shown in column four for qualitative comparison. The viscosity ratio ($\eta = \nu_l/\nu_g$) is 100 in all simulations. The objective of this paper is to demonstrate that the proposed inclusion of external force term is able to simulate density driven multiphase flow using Gunstensen's color model. The extension of the proposed buoyancy model to 3D LBM is straightforward; thus, the accuracy of model results can be improved with 3D LBM simulations.

3.2. Terminal velocity

Davies and Taylor [64] presented an analytical solution to estimate terminal velocity of bubbles in an infinite medium when $Eo > 40$ and $Mo > 200$ by solving the following equation:

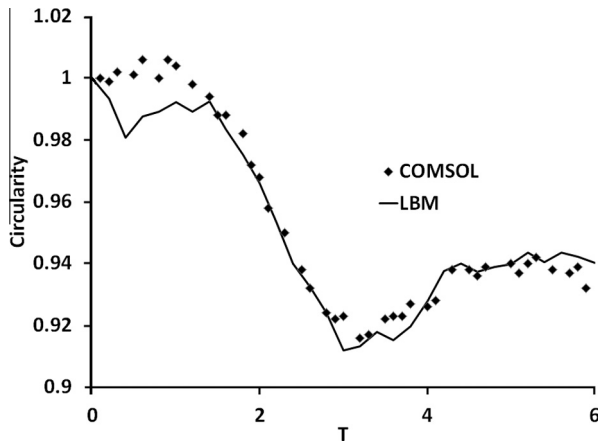


Fig. 6. Change in circularity of bubble with time.

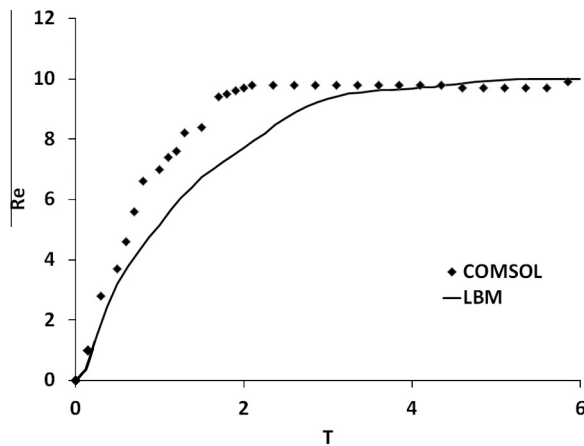


Fig. 7. Change in Re during the rise of bubble.

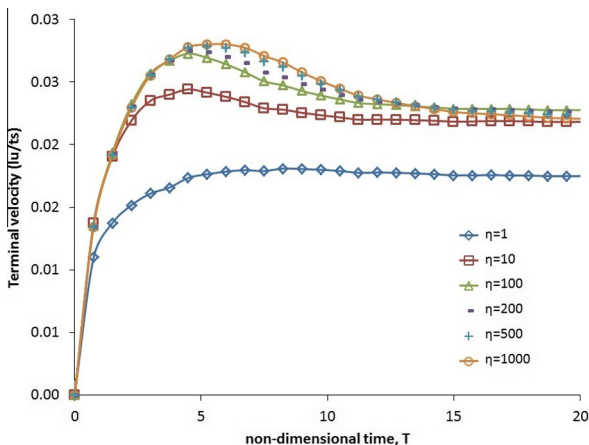


Fig. 8. Effect of viscosity ratio on terminal velocity.

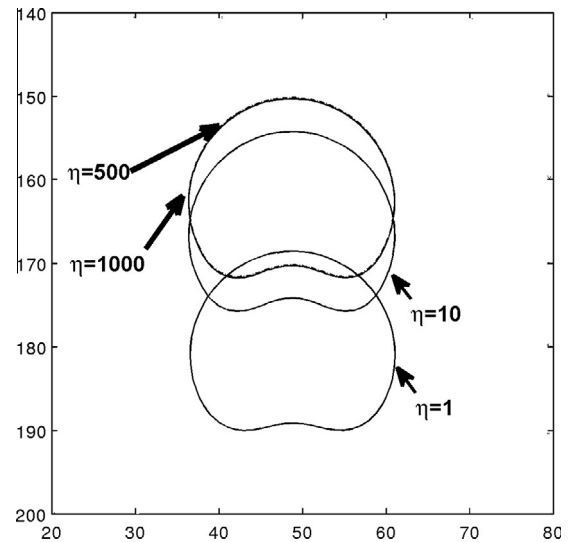


Fig. 9. Effect of viscosity ratio (η) on terminal shape at $T = 12$.

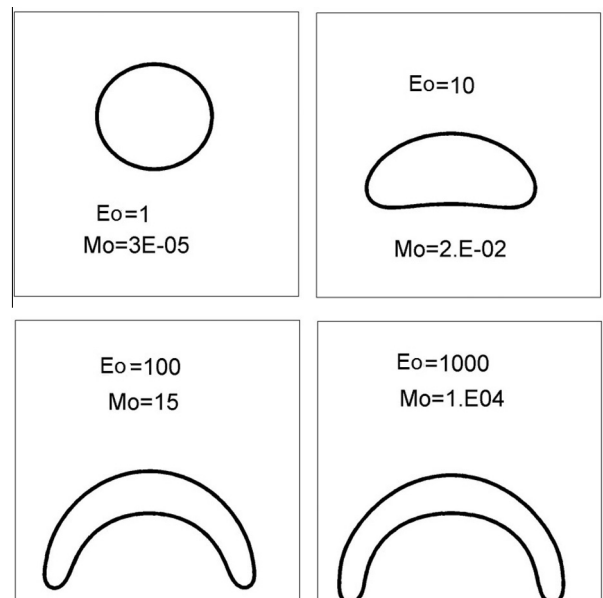


Fig. 10. Terminal shape of bubble at $T = 7$.

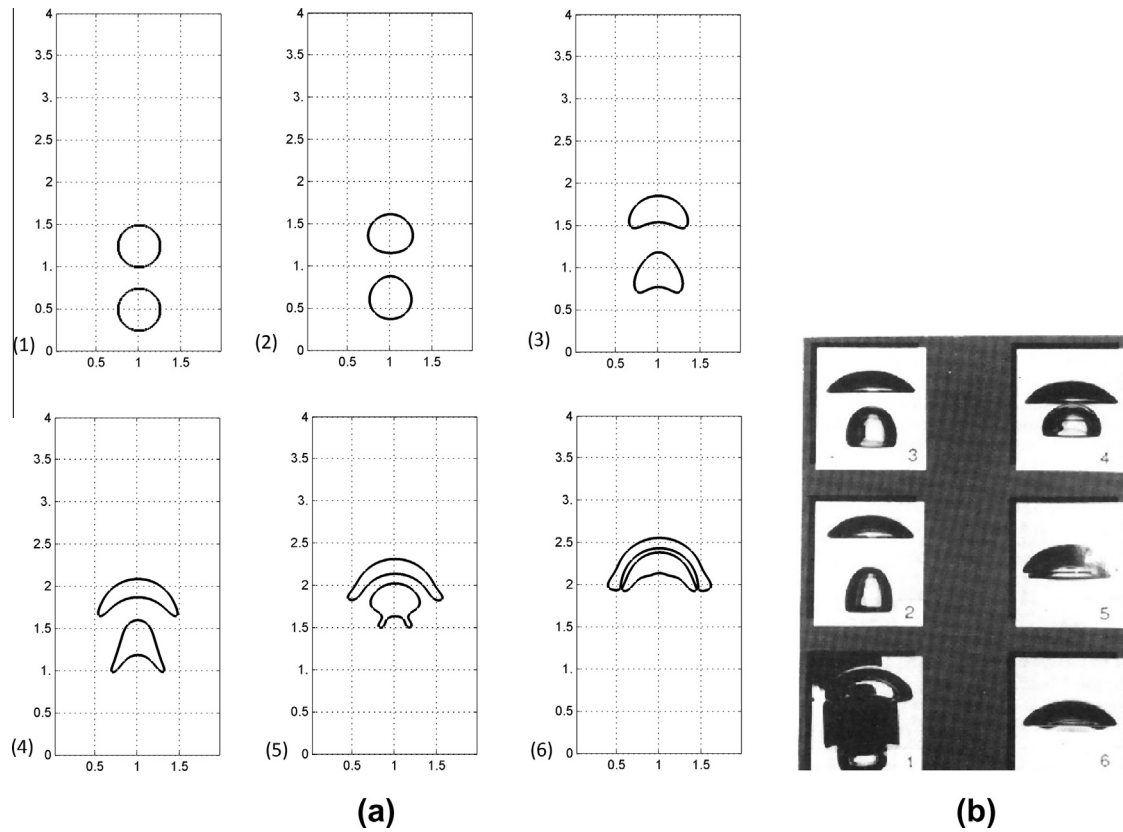


Fig. 11. (a) LBM results of snapshots at different times of the co-axial coalescence of two initially spherical bubbles released from in an initially quiescent liquid at $Eo = 16$ and $M = 2 \times 10^{-4}$. The model time is scaled to match the experimental time scale. (b) The photographs (time difference between subsequent photographs is 0.025 s) taken during experimental observation of coalescence of two co-axial bubbles as given in Brereton and Korotney [65].

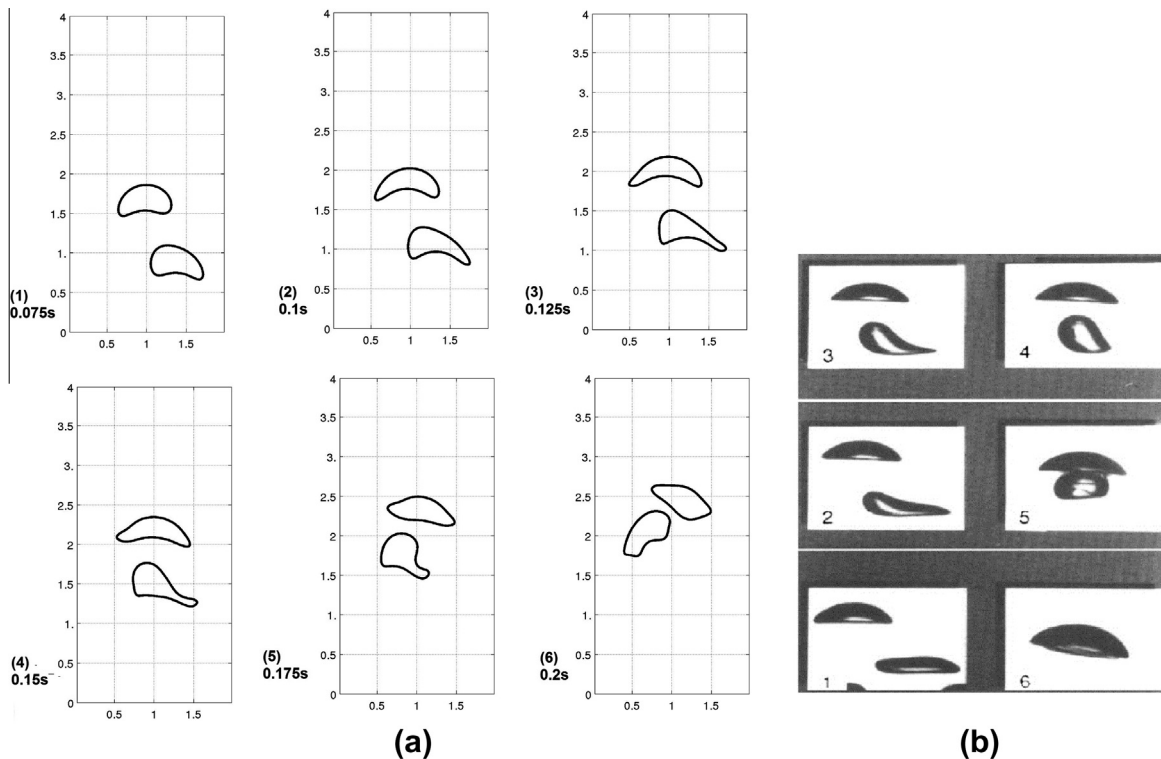


Fig. 12. (a) LBM results of snapshots at different times of the non-co-axial coalescence of two initially spherical bubbles released from in an initially quiescent liquid at $Eo = 16$ and $M = 2 \times 10^{-4}$. The model time is scaled to match the experimental time scale. (b) The photographs (time difference between subsequent photographs is 0.025 s) taken during experimental observation of coalescence of two non-co-axial bubbles as given in Brereton and Korotney [65].

$$2\text{Re}^2 + 6\text{Re} \frac{2+3\eta}{1+\eta} - E_o^{3/2} M_o^{-1/2} = 0.$$

The simulation domain is $96 \text{ lu} \times 288 \text{ lu}$, and the viscosity ratio ($\eta = \nu_l/\nu_g$) is 100. The non-dimensional numbers and LBM parameters are given in Table 2. The comparison between terminal velocity from an LB model and an analytical model is shown in Fig. 4. The model data are in good agreement with the analytical solution.

3.3. Comparison with COMSOL

An LBM simulation of the buoyant rise of bubbles in a domain bounded on all four sides is used for comparison with COMSOL results. A bubble with a diameter of 56 lu is suspended in a domain ($112 \text{ lu} \times 224 \text{ lu}$). The simulation parameters in LBM are such that $E_o = 9$ and $M_o = 6 \times 10^{-4}$. The bubble deforms during the buoyant rise and changes from circular to cap shape. The time steps (ts) in LBM are non-dimensionalized using $T = t_{\text{LBM}} \sqrt{g/d_0}$. The topological change in shape of bubble from LBM simulation at six different non-dimensional time steps (T) is shown in Fig. 5 for a qualitative comparison between LBM and COMSOL results. The qualitative change in the shape of a bubble during the rise of that bubble as predicted by LBM is similar to the results from COMSOL. A more quantitative comparison between two numerical models (LBM and COMSOL) is shown in Figs. 6 and 7 where change in circularity (ξ) of bubble and Re are compared respectively. The circularity (ξ) of bubble is defined as $\xi = \text{perimeter of area equivalent to circle} / \text{perimeter of bubble}$. The LBM simulation results for circularity of bubble and Re are similar to COMSOL results. Similar results for circularity of bubble and Re are shown in Ngachin [32].

3.4. Effect of viscosity ratio

Effect of viscosity contrast between fluid and gas bubble is examined by series of simulations. Six cases of viscosity contrast ($\eta = \nu_l/\nu_g$) = 1, 10, 100, 200, 500, 1000 are simulated and terminal velocity is estimated for each case. Shear stress becomes more significant and interface becomes less mobile at low viscosity contrast. The effect of viscosity ratio on terminal velocity is apparent in Fig. 8. As the viscosity contrast increases the terminal velocity tends to merge into a single curve. The terminal shape of different bubbles for various viscosity ratios is shown in Fig. 9. The terminal shape of bubble does not change significantly at $\eta \geq 500$.

3.5. Effect of surface tension

Surface tension is the property of fluid that tries to retain the spherical shape of the bubble, and it is defined as energy per unit area. We investigated the effect of surface tension on the shape of bubble by changing the E_o number. The surface tension decreases as the E_o number increases, and thus, bubble will more likely deform at higher E_o numbers. We simulated bubble deformation at four E_o numbers where $E_o = 1, 10, 100, 1000$. M_o was changed to maintain a fixed Re . The final shape of the bubble at $T = 7$ is shown in Fig. 10, which look qualitatively similar to results presented by Amaya-Bower and Lee [36]. The terminal shape of bubble remains spherical when $E_o = 1$. The bottom of the bubble is deformed where $E_o = 10$ and it looks like a cap; whereas at higher E_o numbers, e.g., $E_o = 100$ or 1000 , the bubble became more deformed and looked like a skirt. The skirt looked even wider, bigger and taller when $E_o = 1000$.

3.6. Multiple bubbles

The coalescence of two bubbles rising under buoyant force is characterized by three distinct stages. The first stage is when the

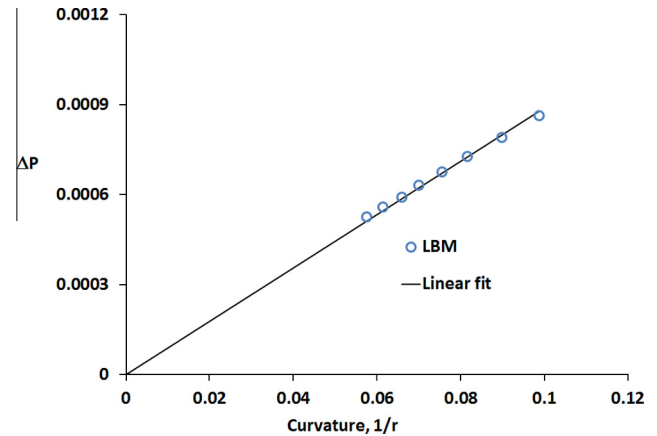


Fig. 13. Curvature of a bubble is plotted against pressure difference to verify surface tension from LBM model against the Laplace's law.

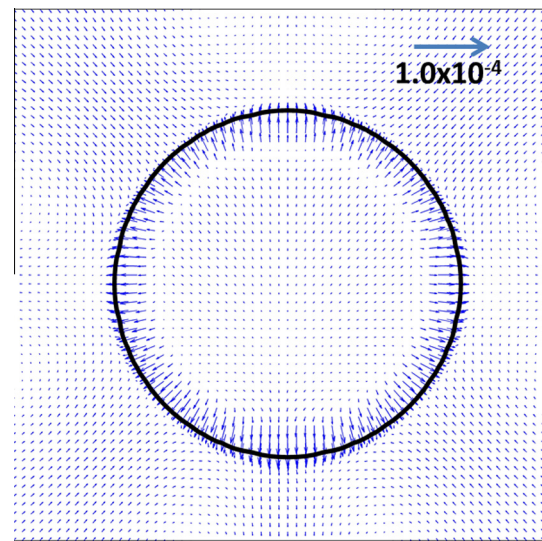


Fig. 14. The spurious velocity near the interface is shown for a bubble of diameter 36 lu surrounded by another fluid (blue). The surface tension (σ) is 0.01 mu/ts^2 . The reference vectors for the spurious velocities are shown for visual guidelines only. (For interpretation of the references to colour in this figure legend, the reader is referred to the web version of this article.)

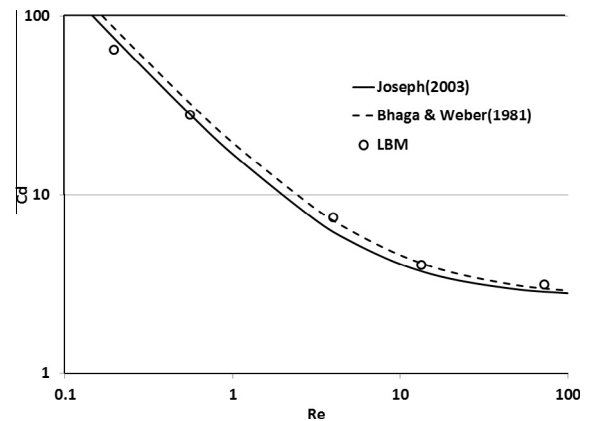


Fig. 15. drag coefficient (C_D) from LBM simulation is compared against theoretical solutions for different Re .

two bubbles approach and a thin liquid film is formed between them. The second stage is when the thickness of liquid film drains

or reduces under capillary and gravitational forces, while the third stage is when the two bubbles coalesce. Brereton and Korotney [65] experimentally photographed the coalescence of two bubbles in two different cases: (1) when the bubbles were initially placed coaxially and (2) when the bubbles were initially placed in an oblique position. The three stages of coaxial coalescence for axial- and oblique-placed bubbles are shown in Figs. 11b and Fig. 12b respectively. The snapshots in Figs. 11b and Fig. 12b are taken at an interval of 0.025 s.

We present LBM simulations where two bubbles are rising in an initially quiescent domain. The initial diameter (d_0) of both bubbles in LBM simulation is 24 lu. The first simulation demonstrates coalescence of two bubbles which were initially aligned axially. The two bubbles were initially separated by $1.5d_0$. The evolution of topographical change in each bubble is compared against the photographs of experimental observations [65] in Fig. 11. The LBM simulation parameters are designed such that non-dimensional numbers $Mo = 2 \times 10^{-4}$ and $Eo = 16$. The Terminal Re should be 45 according to the experiment (Fig. 11b) and the LBM model predicts a terminal Re of 40. The wake created by the leading bubble deforms the trailing bubble and causes the coalescence of two bubbles. The LBM simulation was able to capture the three phases of coalescence for the two bubbles. The time steps in LBM are non-dimensionalized using $T = t_{LBM} \sqrt{g/d_0}$ to match with the experimental results.

The second example demonstrates an LBM simulation of oblique coalescence of two bubbles in an initially quiescent liquid. The bubbles were initially separated by $1.6d_0$ in the vertical direction and $0.8d_0$ in the horizontal direction. The evolution of topographical changes in the test bubble is compared against the photographs of experimental observations [65] in Fig. 12b. The non-dimensional numbers Mo and Eo are 2×10^{-4} and 16 respectively. Similar to the co-axial case (Fig. 11), the leading bubble behaves independently of the trailing bubble. The trailing bubble undergoes significant topological change after entering the wake region behind the leading bubble. This also causes the trailing bubble to coalesce with the leading bubble.

4. Conclusion

A modification in Lattice Boltzmann model (LBM) based on Gunstensen's binary color model is presented to simulate bubble dynamics due to density dependent multiphase flow. The robustness of the model is tested for a range of viscosity ratios (η) and surface tensions (σ) under applied buoyant force due to density contrast between the two fluid components. The terminal velocity seems to be dependent on the viscosity contrast where $\eta < 500$. As viscosity ratio decreases, interface becomes more immobile and shear stress is high. Therefore, the bubble suffers less deformation, and the terminal velocity is reduced. The buoyancy model is verified against the analytical solution for terminal velocity of bubbles at different Eötvös numbers (Eo). The present study shows that the increase of Eo reduces the surface tension; therefore, higher deformation is exhibited by the bubble at a higher Eo number. The model is further verified by comparing the shape of the bubble for a range Eo and Morton numbers (Mo) against the experimental data. The model is verified against the observed experimental data for co-axial and oblique coalescence of two bubbles. This established the verification of an LBM-based buoyant multiphase flow model to simulate density dependent flow of a binary mixture of fluids.

Acknowledgements

The author is grateful to anonymous reviewers and editorial board for the critical reading of the manuscript and much advice. SA would like to acknowledge the GPU computing support from Geo-computing lab in Department of Geology at University of

South Florida Tampa. SA is grateful to Dr. Amit Gupta for help with the development of computer program.

Appendix A

A.1. Laplace's law and interfacial tension

The Laplace's law is an important benchmark test for any multiphase flow model. The interfacial tension between two fluids can be determined using Laplace's law. In 2-D simulation, an initial condition where a gas bubble (g) of different square areas surrounded by the liquid (l) was set up. A circular bubble of gas forms at steady state. The radius of bubble (R) and the pressure difference (Δp) between the inside and outside of the bubble at steady state provides the information needed to construct a linear plot based on the Laplace's law. $\Delta p = p_l - p_g = c \frac{\sigma}{R}$ ($c = 1$ for 2D) where σ (interfacial surface tension) is the slope of linear plot between $1/R$ and Δp . A linear fit (zero intercept) for simulation data is shown in Fig. 13. The interfacial surface tension ($\sigma = 0.01$ mu/ts²) is an input parameter in the Gunstensen's color model and can be set apriori. Similar results were obtained for viscosity ratios (η) between 1 and 100. The error in surface tension (σ) obtained from LBM is within 5–10% of the macroscopic surface tension predicted by the Laplace's law, which has also been shown by Lishchuk et al. [58].

A.2. Static bubble test

Spurious velocities of small but finite magnitude have been observed near the interface of two fluid phases in several LBM based multiphase flow models [66–68]. These spurious velocities must be of negligible magnitude before LBM can be applied for solving real-life engineering problems. A numerical simulation of static bubble was performed in a $96 \text{ lu} \times 96 \text{ lu}$ domain to test the stability of Gunstensen's color model. The initial diameter of bubble surrounded by fluid was 36 lu. The maximum spurious velocity near the interface, between the bubble and the fluid, at equilibrium is 1×10^{-4} lu/ts as shown in Fig. 14. The maximum velocity vector near the interface for the same simulation obtained from Shan–Chen model was 0.1 lu/ts [19]. Later, Shan [66] introduced a method to achieve highly isotropic gradient operators on a lattice to minimize the spurious current in the original Shan–Chen model. Hence, the spurious velocities developed near the interface are negligible for Gunstensen's color model.

A.3. Drag coefficient

Any object moving across the fluid medium experiences a drag force due to pressure and shear force on the surface. The drag coefficient (C_D) is the ratio of the drag force to the force produced by the dynamic pressure times the area. An empirical relationship between C_D and Re is given by Bhaga and Weber [62] for fluids with a high Morton number ($Mo > 4 \times 10^{-3}$)

$$C_D = \left[(2.67)^{0.9} + \left(\frac{16}{Re} \right)^{0.9} \right]^{1/0.9} \quad (10)$$

Joseph [69] theoretically developed drag coefficient (C_D) as:

$$C_D = 0.445 \left(6 + \frac{32}{Re} \right) \quad (11)$$

The LBM simulations for buoyant rise of bubbles are used to estimate drag coefficient (C_D) for a range of Re. The C_D for a rising bubble in a 2D flow system is $C_D = \frac{\pi}{2} \frac{\Delta \rho}{\rho_l} \frac{gd_e}{V^2}$, V is terminal velocity of the bubble, and d_e is the effective diameter of the bubble after deformation during buoyant rise. The comparison between the theoretical

solutions (Eqs. (10) and (11)) and LBM simulation results for drag coefficient (C_D) are shown in Fig. 15. The LBM results for drag coefficient (C_D) are in good agreement with the theoretical solutions.

References

- [1] Wu H-C, Lin H-J, Kuo Y-C, Hwang W-S. Simulation of droplet ejection for a piezoelectric inkjet printing device. *Mater Trans* 2004;45:893–9.
- [2] Siregar DP. Numerical simulation of evaporation and absorption of inkjet printed droplets. 2012.
- [3] Sarkar M. Multiphase flow modeling of spray cooling to improve heat transfer. ProQuest; 2008.
- [4] Selvam RP, Lin L, Ponnappan R. Computational modeling of spray cooling: current status and future challenges. In: AIP Conference Proceedings; 2005. p. 55.
- [5] Bandara UC, Tartakovsky AM, Palmer BJ. Pore-scale study of capillary trapping mechanism during CO₂ injection in geological formations. *Int J Greenhouse Gas Control* 2011;5:1566–77.
- [6] Adenekan A, Patzek T, Pruess K. Modeling of multiphase transport of multicomponent organic contaminants and heat in the subsurface: numerical model formulation. *Water Resour Res* 1993;29:3727–40.
- [7] Armstrong J, Frind E, McClellan R. Non-equilibrium mass transfer between the vapor, aqueous, and solid phases in unsaturated soils during vapor extraction. *Water Resour Res* 1994;30:355–68.
- [8] Fischer U, Schulin R, Keller M. Experimental and numerical investigation of soil vapor extraction. *Water Resour Res* 1996;32:3413–27.
- [9] Pollock DW. Simulation of fluid flow and energy transport processes associated with high-level radioactive waste disposal in unsaturated alluvium. *Water Resour Res* 1986;22:765–75.
- [10] Ahlstrom S, Foote H, Arnett R, Cole C, Serne R. Multicomponent mass transport model: theory and numerical implementation (discrete-parcel-random-walk version). Richland, Wash (USA): Battelle Pacific Northwest Labs.; 1977.
- [11] Prosperetti A, Tryggvason G. Computational methods for multiphase flow. Cambridge University Press; 2007.
- [12] Fuster D, Agbaglah G, Josserand C, Popinet S, Zaleski S. Numerical simulation of droplets, bubbles and waves: state of the art. *Fluid Dynamics Res* 2009;41:065001.
- [13] van Sint Annaland M, Deen N, Kuipers J. Numerical simulation of gas bubbles behaviour using a three-dimensional volume of fluid method. *Chemical Eng Sci* 2005;60:2999–3011.
- [14] van Sint Annaland MW, Deen Dijkhuizen, NG, Kuipers JAM. Numerical simulation of behavior of gas bubbles using a 3-D front-tracking method. *Am Inst Chem Eng* 2006;52:99–110.
- [15] Olsson E, Kreiss G. A conservative level set method for two phase flow. *J Comput Phys* 2005;210:225–46.
- [16] Nagrath S, Jansen KE, Lahey Jr RT. Computation of incompressible bubble dynamics with a stabilized finite element level set method. *Comput Meth Appl Mech Eng* 2005;194:4565–87.
- [17] Deshpande KB, Zimmerman WB. Simulation of interfacial mass transfer by droplet dynamics using the level set method. *Chem Eng Sci* 2006;61:6486–98.
- [18] COMSOL A. COMSOL multiphysics user's guide. Version: September. 2005.
- [19] Gupta A, Kumar R. Lattice Boltzmann simulation to study multiple bubble dynamics. *Int J Heat Mass Transf* 2008;51:5192–203.
- [20] Gunstensen AK, Rothman DH, Zaleski S, Zanetti G. Lattice Boltzmann model of immiscible fluids. *Phys Rev A* 1991;43:4320.
- [21] Inamuro T, Ogata T, Tajima S, Konishi N. A lattice Boltzmann method for incompressible two-phase flows with large density differences. *J Comput Phys* 2004;198:628–44.
- [22] Shan X, Chen H. Lattice Boltzmann model for simulating flows with multiple phases and components. *Phys Rev E* 1993;47:1815.
- [23] Shan X, Doolen G. Multicomponent lattice-Boltzmann model with interparticle interaction. *J Statist Phys* 1995;81:379–93.
- [24] Swift MR, Osborn W, Yeomans J. Lattice Boltzmann simulation of non-ideal fluids. *Phys Rev Lett* 1995;75:830–3.
- [25] Lee T, Lin CL. A stable discretization of the lattice Boltzmann equation for simulation of incompressible two-phase flows at high density ratio. *J Comput Phys* 2005;206:16–47.
- [26] Ahrenholz B, Tölke J, Lehmann P, Peters A, Kaestner A, Krafczyk M, et al. Prediction of capillary hysteresis in a porous material using lattice-Boltzmann methods and comparison to experimental data and a morphological pore network model. *Adv Water Resour* 2008;31:1151–73.
- [27] Gunstensen AK, Rothman DH. Microscopic modeling of immiscible fluids in three dimensions by a lattice Boltzmann method. *EPL (Europhys Lett)* 1992;18:157.
- [28] Rothman DH, Keller JM. Immiscible cellular-automaton fluids. *J Statist Phys* 1988;52:1119–27.
- [29] Swift MR, Orlandini E, Osborn W, Yeomans J. Lattice Boltzmann simulations of liquid–gas and binary fluid systems. *Phys Rev E* 1996;54:5041.
- [30] Huang H, Wang L, Lu X-y. Evaluation of three lattice Boltzmann models for multiphase flows in porous media. *Comput Math Appl* 2011;61:3606–17.
- [31] Sankaranarayanan K, Kevrekidis I, Sundaresan S, Lu J, Tryggvason G. A comparative study of lattice Boltzmann and front-tracking finite-difference methods for bubble simulations. *Int J Multiphase Flow* 2003;29:109–16.
- [32] Ngachin M. Simulation of rising bubbles dynamics using the lattice Boltzmann method. FIU Electronic Theses and Dissertations: Florida International University; 2011.
- [33] Tölke J. Lattice Boltzmann simulations of binary fluid flow through porous media. *Philosophical Trans Roy Soc Lond Ser A: Math Phys Eng Sci* 2002;360:535–45.
- [34] Gupta A, Kumar R. Flow regime transition at high capillary numbers in a microfluidic T-junction: viscosity contrast and geometry effect. *Phys Fluids* 2010;22:122001.
- [35] Tölke J, Prisco GD, Mu Y. A lattice Boltzmann method for immiscible two-phase stokes flow with a local collision operator. *Comput Math Appl* 2012.
- [36] Amaya-Bower L, Lee T. Single bubble rising dynamics for moderate Reynolds number using lattice Boltzmann method. *Comput Fluids* 2010;39:1191–207.
- [37] Takada N, Misawa M, Tomiyama A, Hosokawa S. Simulation of bubble motion under gravity by lattice Boltzmann method. *J Nucl Sci Technol* 2001;38:330–41.
- [38] Kurtoglu IO, Lin CL. Lattice Boltzmann study of bubble dynamics. *Numer Heat Transf Part B: Fund* 2006;50:333–51.
- [39] Farhat H, Choi W, Lee JS. Migrating multi-block lattice Boltzmann model for immiscible mixtures: 3D algorithm development and validation. *Comput Fluids* 2010;39:1284–95.
- [40] Tölke J, Freudiger S, Krafczyk M. An adaptive scheme using hierarchical grids for lattice Boltzmann multi-phase flow simulations. *Comput Fluids* 2006;35:820–30.
- [41] Gupta A, Kumar R. Effect of geometry on droplet formation in the squeezing regime in a microfluidic T-junction. *Microfluidics Nanofluidics* 2010;8:799–812.
- [42] Grunau D, Chen S, Egger K. A lattice Boltzmann model for multi-phase fluid flows. *Arxiv, preprint comp-gas/9303001*. 1993.
- [43] Farhat H, Lee JS, Lee JS. A multi-component lattice Boltzmann model with non-uniform interfacial tension module for the study of blood flow in the microvasculature. *Int J Numer Meth Fluids* 2011;67:93–108.
- [44] Leclaire S, Reggio M, Trépanier J-Y. Numerical evaluation of two recoloring operators for an immiscible two-phase flow lattice Boltzmann model. *Appl Math Modell* 2012;36:2237–52.
- [45] Latva-Kokko M, Rothman DH. Diffusion properties of gradient-based lattice Boltzmann models of immiscible fluids. *Phys Rev E* 2005;71:056702.
- [46] Li X, Zhang Y, Wang X, Ge W. GPU-based numerical simulation of multi-phase flow in porous media using multiple-relaxation-time lattice Boltzmann method. *Chem Eng Sci* 2013.
- [47] Sankaranarayanan K, Shan X, Kevrekidis KGS. Bubble flow simulations with the lattice Boltzmann method. *Chem Sci Eng* 1999;54:4817–23.
- [48] Yu Z, Fan L-S. An interaction potential based lattice Boltzmann method with adaptive mesh refinement (AMR) for two-phase flow simulation. *J Comput Phys* 2009;228:6456–78.
- [49] Inamuro T, Ogata T, Ogino F. Numerical simulation of bubble flows by the lattice Boltzmann method. *Future Gen Comput Syst* 2004;20:959–64.
- [50] Inamuro T, Tajima S, Ogino F. Lattice Boltzmann simulation of droplet collision dynamics. *Int J Heat Mass Transf* 2004;47:4649–57.
- [51] Zheng H, Shu C, Chew Y. A lattice Boltzmann model for multiphase flows with large density ratio. *J Comput Phys* 2006;218:353–71.
- [52] Mohamad A, Kuzmin A. A critical evaluation of force term in lattice Boltzmann method, natural convection problem. *Int J Heat Mass Transf* 2010;53:990–6.
- [53] Buick J, Greated C. Gravity in a lattice Boltzmann model. *Phys Rev E* 2000;61:5307.
- [54] Succi S. The lattice Boltzmann equation. *Fluid Dynamics Beyond* 2001.
- [55] Chen S, Doolen GD. Lattice Boltzmann method for fluid flows. *Ann Rev Fluid Mech* 2003;30:329.
- [56] Qian Y, d'Humieres D, Lallemand P. Lattice BGK models for Navier–Stokes equation. *EPL (Europhys Lett)* 1992;17:479.
- [57] Bhatnagar PL, Gross EP, Krook M. A model for collision processes in gases. I. Small amplitude processes in charged and neutral one-component systems. *Phys Rev* 1954;94:511.
- [58] Lischuk S, Care C, Halliday I. Lattice Boltzmann algorithm for surface tension with greatly reduced microcurrents. *Phys Rev E* 2003;67:036701.
- [59] Noble DR, Chen S, Georgiadis JG, Buckius RO. A consistent hydrodynamic boundary condition for the lattice Boltzmann method. *Phys Fluids* 1995;7:203.
- [60] Grace J. Shapes and velocities of bubbles rising in infinite liquids. *Trans Inst Chem Eng* 1973;51:116–20.
- [61] Clift R, Grace JR, Weber ME. Bubbles drops and particles. New York: Academic Press; 1978.
- [62] Bhaga D, Weber M. Bubbles in viscous liquids: shapes, wakes and velocities. *J Fluid Mech* 1981;105:61–85.
- [63] Hua J, Lou J. Numerical simulation of bubble rising in viscous liquid. *J Comput Phys* 2007;222:769–95.
- [64] Davies R, Taylor G. The mechanics of large bubbles rising through extended liquids and through liquids in tubes. *Proc Roy Soc Lond Ser A Math Phys Sci* 1950;200:375–90.
- [65] Brereton G, Korotney D. Coaxial and oblique coalescence of two rising bubbles. Dynamics of bubbles and vortices near a free surface. *AMD*; 1991. p. 119.
- [66] Shan X. Analysis and reduction of the spurious current in a class of multiphase lattice Boltzmann models. *Phys Rev E* 2006;73:047701.
- [67] Cristea A, Sofonea V. Reduction of spurious velocity in finite difference lattice Boltzmann models for liquid–vapor systems. *Int J Modern Phys C* 2003;14:1251–66.
- [68] Wagner AJ. The origin of spurious velocities in lattice Boltzmann. *Int J Modern Phys B* 2003;17:193–6.
- [69] Joseph DD. Rise velocity of a spherical cap bubble. *J Fluid Mech* 2003;488:213–23.
- [70] Sukop MC, Thorne DT. Lattice Boltzmann modeling: an introduction for geoscientists and engineers. Springer Verlag; 2006.